

UHF RFID Tag Antenna-Based Sensing for Corrosion Detection & Characterization Using Principal Component Analysis

Jun Zhang, *Member, IEEE* and Gui Yun Tian, *Senior Member, IEEE*

Abstract—Recently, structural health monitoring (SHM) using radio frequency identification (RFID) tag antenna-based sensing (TABS) has received increasing attention because of its wireless, passive, and low-cost characteristics. However, a great challenge in the SHM using RFID TABS is multiple influences in the measurement. This paper presents an ultra-high frequency (UHF) RFID sensor system for corrosion detection and characterization. In this study, a 3-D antenna sensor is designed to work on the surface of a protective coated steel sample. Sweep-frequency measurements are applied for analog identifier (AID) with principal component analysis (PCA) to overcome the multiple influences from reader-tag orientation, distance, and environment. Feature extraction and selection through PCA can get robust and sensitive defect information by projecting the test data into an orthogonal feature space. The test results demonstrate that the proposed method can be applied to detect and characterize early-stage corrosion in metals.

Index Terms—Antenna sensor, principal component analysis (PCA), corrosion detection, radio frequency identification (RFID), structural health monitoring (SHM).

I. INTRODUCTION

Structural health monitoring (SHM) and structural integrity evaluation (SIE) based on radio frequency identification (RFID) in the ultra-high frequency (UHF) band are receiving more and more attention because of their wireless, passive, and low-cost characteristics. Integrating sensing ability in RFID tags renders the whole system capable of not only tracking, but also providing real-time cognition of aspects of object's status or environmental conditions [1], [2]. Recently, people's readiness to use RFID based "smart skin" for in situ monitoring of the health state of large-scale infrastructure is increasing, thanks to the low cost and wide availability of RFID technology [3].

The last several decades have witnessed unprecedented prosperity in railway industry globally. Potential threats behind

such a rapid expansion of railway network must be envisaged [4]. The surface of the rail web (cross section connecting the rail head with the foot) and foot (base support of the rail) can be wasted by corrosion, leading to fracture and derailment [5], which will finally jeopardize the safety. Detection and characterization of corrosion is of paramount importance in railway track for safety and reliability of operation and maintenance. In contrast to conventional approaches of corrosion characterization considered as "metal loss", e.g. thickness changes [6], early-stage corrosion can be characterized by pitting corrosion [7], which leads to an increase in the surface roughness and reduction in the conductivity and permeability [8]. Electromagnetic (EM) non-destructive testing and evaluation (NDT&E) methods, such as pulsed eddy current [8], eddy current pulsed thermography (ECPT) [9], and microwave waveguide [10], can be used to detect and evaluate the corrosion. The experimental results have illustrated that these EM NDT&E methods are very effective to detect, evaluate, and predict the coated corrosion. However, it is difficult for these methods to permanently monitor corrosion due to the complex and bulky systems. Therefore, it is timely demanding to develop EM sensors that can be used to sense corrosion in order to undertake long-term/permanent-installed SHM and SIE. For railway monitoring, a large deployment of low-cost sensors is required owing to the large-scale structure. This makes passive RFID a good candidate among in situ, on-demand, and remote monitoring techniques [11].

Low frequency (LF) [12] and high frequency (HF) [13] RFID tag antenna based sensing (TABS) were explored for detecting and characterizing corrosion under paint and insulation. Because of magnetic coupling (evanescent mode), the detection distance between LF/HF RFID tag and reader is quite short (in the range of several centimeters). UHF RFID TABS can be used to increase the monitoring distance resulting from EM coupling (radiation mode) [14]. The challenges of RFID sensor system for remotely monitoring the defects of metallic objects need to address the design and development of a metal-mountable antenna for both sensing and communication, to remote access for data collection (interrogation) with good signal-to-noise ratio (SNR) subjected to environment interference, and to extract features for

Manuscript received October 6, 2015, revised May 11, 2016, accepted 4 June, 2016. This work was supported by the Novel Sensing Network for Intelligent Monitoring (NEWTON) project of EPSRC.

Jun Zhang and Gui Yun Tian are with School of Electrical and Electronic Engineering, Newcastle University, Newcastle upon Tyne, NE1 7RU, United Kingdom (e-mail: jun.zhang@newcastle.ac.uk; g.y.tian@newcastle.ac.uk).

information required [15], [16]. Detailed challenges and progress of RFID antenna sensors and systems can be discussed below.

Contrary to the traditional metal-mountable antenna design, TABS takes advantage of the change underneath the tagged metallic objects [17]. The recent attempts to use UHF RFID tag antennas to monitor defects can be categorized into two main families: direct changes of antenna physical parameters and indirect changes of antenna property. For the former case, a flexible meander-line dipole was developed to monitor the strain with a sub-millimeter resolution [18]. The ink-jet printing [19] or embroidery technology [20] was applied to reduce the cost or improve the performance of strain sensors. However, the resolution and dynamic range of such type of antennas may be influenced by each other. For the latter case, a microstrip antenna sensor was developed to monitor the growth of cracks with a sensitivity of 22 MHz/mm [21]. Moreover, a dual-resonant (TM01 and TM10 modes) microstrip antenna was proposed to detect the orientation of cracks and demonstrated that its sensitivity was related to the relative permittivity and geometrical length [22]. Further information about TABS can be found in [23].

The radio frequency (RF) signals carrying sensed information are backscattered into the wireless channel and RFID antenna sensors with the combination of sensing and communication in the system need addressing the RF channel to mitigate path loss and multipath effects [24]. In a multipath environment, backscatter RFID systems suffer from small-scale fading effects [25], which are more severe than in classical one-way systems. The backscattered signal is subject to environmental multipath en route reader that causes both frequency and time-selective effects [26]. As a result, multi-antenna techniques in RFID based systems have come into the focus of research to overcome this drawback [27]. This technology increases the design and manufacturing costs. Since backscattered power varies depending on the distance separation between the reader and the tag, a reference tag was used for differential measurement [28]. Without a priori information about the tag-reader mutual position, multiple measurements can be applied for separation and reduction of multiple influence. An analog identifier (*AID*) was invented for this purpose [29], which has been proved that *AID* is preferred among power metrics in terms of repeatability [30]. Benefited from a large variation of the tag chip impedance (nonlinearity), the influence from the environment may be mitigated by a double-power measurement technique [20].

The reader can continuously monitor the measurable parameters, e.g. forward power and backscatter power, and then features such as resonant frequency shift (RFS) can be extracted and used to detect and characterize the defect. However, in the RFID sensor system, the contributions of the multi-parameter from the defect mix with multiple influences from the environment. To this end, principal component analysis (PCA) and independent component analysis (ICA) based pattern recognition algorithms can be used to extract the dominant variance and statistically separate the sensed signal

from the interference, which has been applied in the field of NDT&E to analyze data from pulsed eddy current testing for detecting metal loss [31], cracks in multi-layer structures [32], and corrosion [33]. More recently, PCA has been used to study the multi-parameter effects of stress and defects in ECPT [34].

This paper is to address the challenges of detecting and characterizing corrosion in metals using RFID sensor system in terms of antenna design, system configuration, feature extraction and corrosion characterization. A three-dimensional (3-D) metal mountable tag antenna is proposed to optimize the trade-off between sensing and communication. PCA is utilized to extract the defect information from multi-parameter signatures of corrosion in sweep-frequency measurements. The rest of this paper is organized as follows. At first, the sensing variable and PCA will be introduced in Section II. In Section III, antenna sensor design will be presented. After that, test setup will be illustrated and the test results using the proposed method will be discussed in Section IV. Finally, conclusions will be drawn and future work will be pointed out.

II. SENSING VARIABLE AND MULTI-PARAMETER ANALYSIS

To develop RFID sensor system for corrosion detection and characterization, research work needs to cover tag antenna design for working on metallic surfaces with reasonable sensitivity and robust (signal) feature extraction for corrosion characterization independent of the interference. The former is left for discussion in the next section while the latter will be discussed in this section.

It is of paramount importance to mitigate multiple influences to get robust sensing information from the RFID sensor system. Several interferences including sample surface geometry, multiple scattering due to nearby objects, and communication distance between the tag and the reader are mixed and thus need to be separated.

The antenna sensor can sense the defect through the sensing variable, but the interferences change the impedance and radiation pattern of the antenna and therefore force the change in sensing variable as well. An analytical approach is applied to understand the measurable parameters and sensing variables. A robust sensing variable is selected.

At the same time, a mathematical processing that accounts for the effects of multi-parameter signatures of corrosion is proposed. The PCA method with the help of sweep-frequency measurements is utilized to extract the dominant feature from the sensing variable. More details are explained in the next two subsections.

A. Sensing Variable

Under the hypothesis of line-of-sight (LOS) propagation between the reader and tag antennas, the backscattered power in the free space by the Friis formula can be expressed as [35]

$$P_{R \leftarrow T}[\Psi(\theta, \phi)] = \frac{1}{4\pi} \left(\frac{\lambda_0}{4\pi d} \right)^2 \times \times P_{in} G_R^2(\theta, \phi) \eta_p^2 RCS[\Psi(\theta, \phi)] \quad (1)$$

where d is the reader-tag distance, λ_0 is the wavelength, P_{in} is the power transmitted by reader, $G_R(\theta, \phi)$ is the gain of the reader antenna, η_ρ is the polarization mismatch between the reader and tag antennas, and $RCS[\Psi(\theta, \phi)]$ is the radar cross-section of the tag, which depends on [17]

$$RCS[\Psi(\theta, \phi)] = \frac{\lambda_0^2}{4\pi} G_T^2[\Psi(\theta, \phi)] \tau[\Psi] \frac{R_A[\Psi]}{R_L}. \quad (2)$$

Here, Ψ represents the defect variable and $G_T[\Psi(\theta, \phi)]$ is the gain of the tag antenna. At the same time, the forward power to activate tag, i.e. P_{in}^{to} , can be written as

$$P_{in}^{to}[\Psi(\theta, \phi)] = \left(\frac{4\pi d}{\lambda_0} \right)^2 \times \frac{P_{th}}{G_R(\theta, \phi) G_T[\Psi(\theta, \phi)] \tau[\Psi] \eta_\rho}, \quad (3)$$

where P_{th} is the minimum incident power needed to activate the tag chip (also called read sensitivity). The power transmission coefficient, which accounts for the impedance mismatch between the tag chip ($Z_L = R_L + jX_L$) and the tag antenna ($Z_A[\Psi] = R_A[\Psi] + jX_A[\Psi]$), is given by

$$\begin{aligned} \tau[\Psi] &= 1 - |S_{11}[\Psi]|^2 = 1 - \left| \frac{Z_L - Z_A^*[\Psi]}{Z_L + Z_A[\Psi]} \right|^2 \\ &= \frac{4R_LR_A[\Psi]}{|Z_L + Z_A[\Psi]|^2} \leq 1 \end{aligned}, \quad (4)$$

where $Z_A^*[\Psi]$ is the conjugate value of the antenna impedance. The variation of the load impedance Z_L between the values $Z_{L,1}$ and $Z_{L,2}$ (load modulation) produces two different values of the power reflection coefficients ($\tau_1[\Psi]$ and $\tau_2[\Psi]$).

The differential radar cross-section (ΔRCS) of an RFID tag is an important parameter, which determines the power of the modulated backscattered tag signal [36]. The ΔRCS can be expressed as [37]

$$\Delta RCS[\Psi(\theta, \phi)] = \frac{\lambda_0^2}{4\pi} G_T^2[\Psi(\theta, \phi)] |\tau_1[\Psi] - \tau_2[\Psi]|^2 \quad (5)$$

for both amplitude-shift-keying (ASK) and phase-shift-keying (PSK) modulation. By means of ad hoc test-beds, it has been demonstrated that backscattered power exhibits a combined uncertainty ranging from 0.5 to 2 dB, with a deep dependence on the measurement instrumentation [30].

The measurement of ΔRCS suffers from the mutual distance and orientation between the reader and tag antennas. To address this issue, an indirect measurable parameter, independent of the reader-tag mutual position and orientation [35], can be obtained by combining the forward power (eq. (3)) and the backscattered power (eq. (1))

$$\begin{aligned} AID[\Psi] &= \frac{P_{th}}{\sqrt{P_{in}^{to}[\Psi(\theta, \phi)] P_{R \leftarrow T}[\Psi(\theta, \phi)]}} \\ &= \frac{2R_L}{|Z_A[\Psi] + Z_L|}. \end{aligned} \quad (6)$$

In eq. (6), $P_{R \leftarrow T}$ is the corresponding backscattered power in the tag's absorbing state when P_{in}^{to} is the turn on power. $P_{R \leftarrow T}$ can be gathered, in principle, by the differential backscattered powers in the absorbing and reflecting states [17], or received signal strength indicator (RSSI).

Comparing with $P_{R \leftarrow T}$, P_{in}^{to} , and ΔRCS , AID has a robust feature due to the ratio of power that is only related to impedance rather than antenna gain [15].

B. Multi-parameter Analysis

The sensing mechanism of the UHF RFID TABS is similar to the pulsed eddy current technique [8], which uses alternating magnetic (evanescent) field to generate eddy current and then interacts with the sample. The surface roughness, thickness, conductivity, and permeability of steel and corroded area contribute to the variation of the tag antenna's impedance.

To simplify the analysis, the observation matrix is assumed to be a mixture of several sources, additive scatter, and noise with mixing weight, m_i ($i = 1, 2, 3, 4$). The mathematical definition of the mixing model can be described as

$$Y = \sum_{i=1}^{N_s} m_i X_i + S + N, \quad (7)$$

where $N_s = 4$ denotes the number of sources. $X_{1,2,3,4}(f)$ refers to the defect variable (Ψ), including thickness, surface roughness, conductivity, and permeability of corrosion layer and steel. $S(f)$ refers to the scatter caused by nearby objects and $N(f)$ represents noise, e.g. phase noise of the reader [38].

The first term of eq. (7) is bearing the multi-parameter defect information. The second term, nearby objects in the reader or tag, leads to an uncertainty in the measurement of forward and backscattered powers [39].

PCA is utilized to extract the dominant feature. The details of data processing method used in this paper are depicted in the following steps [40]:

1. Organize the data set as an $N \times M$ matrix, where N is the number of corrosion samples used and M is the number of the frequency points of the sweep-frequency measurement.
 2. Normalize the data to have zero mean and unity variance.
 3. Calculate the eigenvectors–eigenvalues of the covariance matrix by Singular Value Decomposition (SVD).
 4. Select the first and second eigenvectors corresponding to the first and second largest eigenvalues as the first principal component (PC1) and second principal component (PC2).
 5. Transform the original data onto the selected PCs and obtain the corresponding projection coefficients (Ω_i).
- Ω_1 and Ω_2 are selected as the new features, which represent the projections of $AIDs$ onto the PC1 and PC2, respectively.

By projecting the measurement quantity into an orthogonal space spanned by the eigenvectors of the covariance matrix corresponding to the maximum variability within the data, PCA is used to extract the dominant variance from multi-parameter signatures of the defect, to mitigate multiple effects from nearby objects, and to reduce the noise.

III. ANTENNA SENSOR DESIGN

In the previous section, we analyzed a robust sensing variable and feature extraction method. To design specific antenna with a reasonable sensitivity and communication distance, the physical, chemical, and electrical properties of the corrosion sample need to be taken into consideration. With the help of simulation, this section presents the EM modeling of corrosion stages, the design rule of a prototype antenna sensor, and the optimization procedure to balance the trade-off between sensing and communication.

A. Sample Preparation

Corrosion in steel is a general term for a series of iron oxides (hematite α -Fe₂O₃, magnetite Fe₃O₄, and maghemite γ -Fe₂O₃) and hydroxides (ferrous hydroxide Fe(OH)₂, ferric hydroxide Fe(OH)₃, and goethite α -FeOOH), and over time only the proportions of the corrosion constituents change, there is little effect on the composition [8].

According to [41], the electrical conductivity and relative permeability of steel are 4.68×10^6 S/m and 60 while the electrical conductivity and relative permeability of corrosion are about 0.75×10^6 S/m and 4, respectively. Therefore, the skin depth is about 0.9 μ m in steel and approximately 9.2 μ m in corroded area at 1 GHz. The effect of the loss from eddy current induced by surface roughness can be neglected if their dimensions are not comparable, on the average, to the skin depth [42]. Because of the increase in the surface roughness, the conductivity of the corroded area will decrease with the corrosion progression.

The samples (mild steel S275) used in this study, with length \times width \times height of 300 mm \times 150 mm \times 3 mm, are provided by International Paint (Fig. 1a), the center part (corroded area with a size of 30 mm \times 30 mm) of which was exposed to a marine atmosphere for a certain time (0, 1, 3, 6, 10, and 12 months) and then covered using a non-conductive paint in a thickness of ~ 100 μ m. For reference convenience, these six-stage samples are respectively represented as *M0*, *M1*, *M3*, *M6*, *M10*, and *M12*. The corrosion samples can be divided into two categories [43]: early stage (*M0*, *M1*, *M3*, and *M6*) and later stage (*M10* and *M12*).

To facilitate early detection and characterization of corrosion, this study focuses on the early-stage ones where pitting corrosion is dominant. At this stage, the corrosion layer thickness (t) increases as corrosion progresses [8]. This parameter becomes an interesting signature to be measured. For simplicity, the covering layer can be treated as a dry-air film and the corrosion sample is therefore modeled as a multi-layered structure, which is depicted in Fig. 1b.

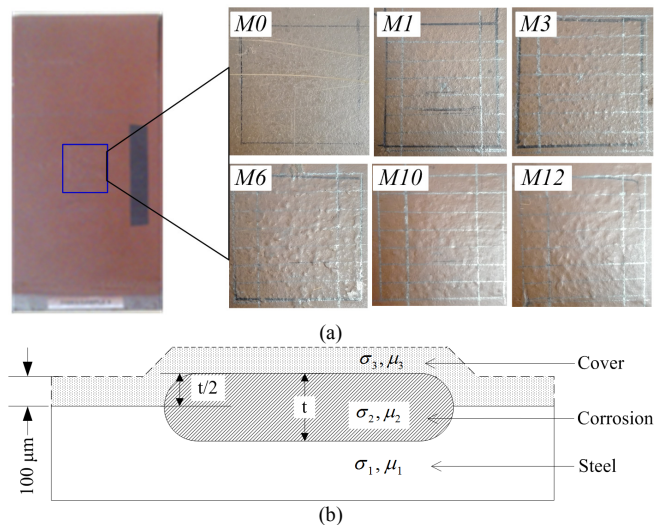


Fig. 1. (a) The corrosion samples in six different stages and (b) the simplified model.

B. Antenna Design for Sensing and Communication

To achieve an optimal trade-off between sensing and communication is a major consideration in the design of an antenna sensor. The proximity coupling between the antenna and the tagged object can be utilized for sensing purpose when disturbance underneath the antenna sensor occurs at a presence of corrosion. The high-quality-factor antenna offers a better sensitivity for sensing, but can be costly to implement and difficult to attach to the surface of a flat metallic structure [44]. Owing the edge effect [45], the antenna size needs to be reduced down to corrosion patch to maximize the sensitivity. For these reasons, the antenna should be electrically small in order to be more sensitive. In addition, the cost consideration in manufacturing requires a simple antenna structure as well as use of lossy substrate materials. This will substantially reduce the communication distance. In complementary, a larger height profile (aspect ratio) is required to enhance the reading performance [46]. This may also lead to a non-directional radiation pattern, allowing tag to be easily identified.

A 3-D cage antenna is proposed to facilitate the size reduction and to be conjugately matched with a capacitive load, i.e. tag chip. The antenna is prototyped for conjugate impedance matching to the passive tag chip of IMPINJ MONZA 4QT in the single-port connection, the input impedance (Z_{in}) and nominal read sensitivity (P_{th}) of which are $11 - j143 \Omega$ and -17.4 dBm at 915 MHz, respectively. The equivalent input impedance of this chip can be treated as a 1.65-k Ω resistor connected in parallel with a 1.21-pF capacitor [47]. An FR4 material, with a loss tangent of 0.02 and a relative permittivity of 4.4, is used in this design. The proposed antenna is shown in Fig. 2a, the substrate of which consists of 10 layers of FR4 lamination, with a standard thickness of 1.6 mm for each layer. The total size of the antenna is 20 mm \times 20 mm \times 16 mm. The reason for the selection of the height profile (h) will be further discussed from sensing point of view in the next part.

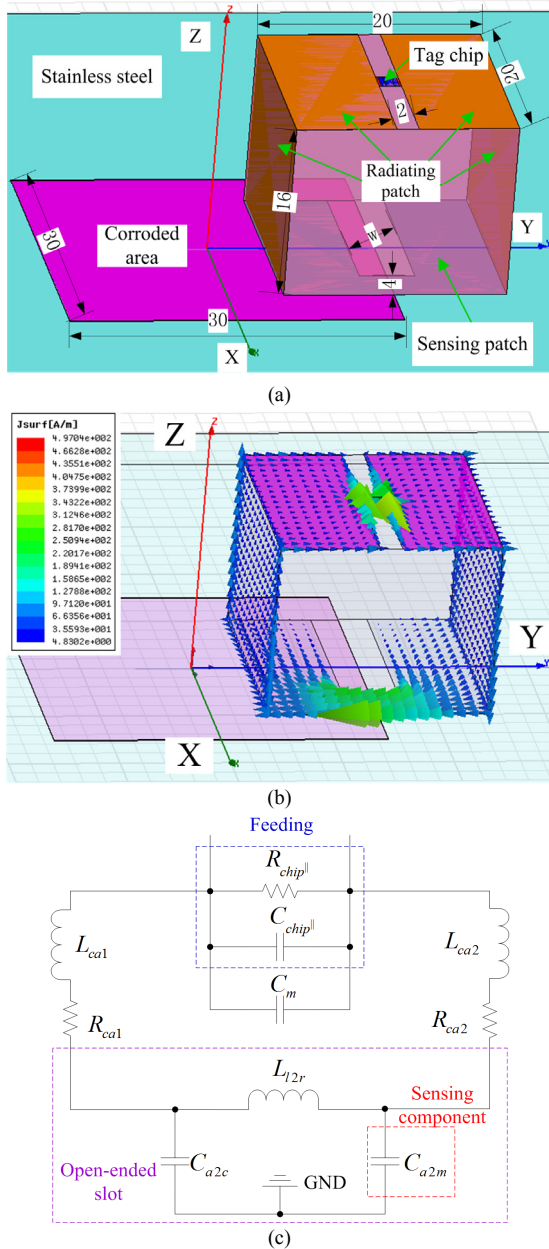


Fig. 2. (a) The proposed 3D metal mountable UHF RFID tag antenna, (b) the simulated current distribution, and (c) the equivalent circuit, where $C_m = 0.57$ pF, $L_{ca1} = 6.81$ nH, $R_{ca1} = 1.08$ Ω , $L_{ca2} = 6.81$ nH, $R_{ca2} = 1.08$ Ω , $C_{a2c} = 14.45$ pF, $L_{12r} = 1.67$ nH, and $C_{a2m} = 15.70$ pF at $w = 5$ mm and $t = 40$ μ m.

To enable the sensing ability for such a tag antenna, an open-ended slot is first etched on the sensing patch, as shown in Fig. 2a. Consequently, an enhancement in the current distribution can be formed near the slot (see Fig. 2b). Second, we deploy the antenna in the edge of corroded area; hence, the corrosion and steel will respectively affect the left and right part of the sensing patch, and thus generates an uneven current distribution in this patch. Since the antenna is directly mounted on the corrosion sample, the distance of the antenna to the corroded area is fixed. Using such a configuration, we can measure the thickness difference between the corrosion layer and the base material (steel).

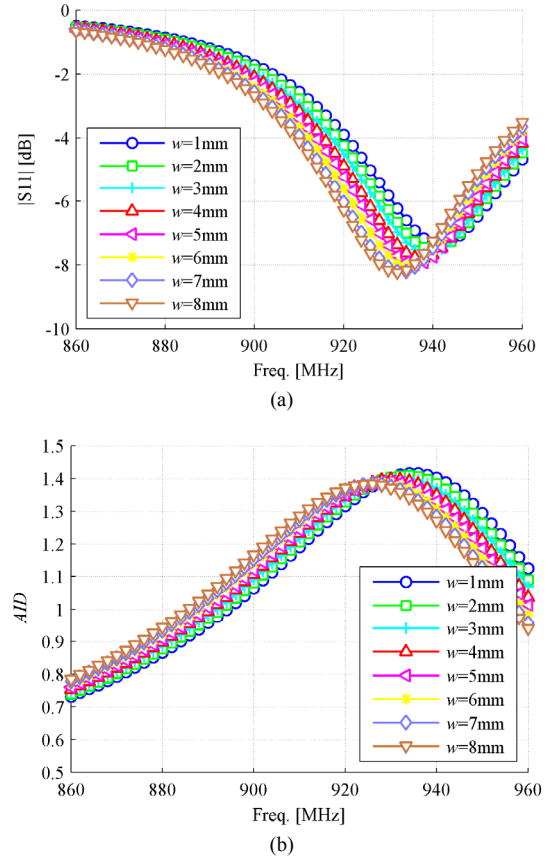


Fig. 3. Simulated (a) reflection coefficients (S_{11}) and (b) $AIDs$ in the variation of w when $t = 40$ μ m.

The lumped circuit analogy is given out in Fig. 2c to gain a physical insight into the operation of the proposed antenna sensor and find the variation of the sensing variable as corrosion progresses. We can generate an equivalent circuit model for the proposed antenna sensor by starting from the cage structure, where the C_m represents the feeding gap, the L_{cax} and R_{cax} ($x = 1, 2$) represent the inductance and resistance (including loss) of the cage structure. The displacement and longitudinal current in the open-ended slot can be respectively modeled by two parallel capacitors and one inductor in series connected in between. The C_{a2c} is to account for the capacitive coupling of the antenna to the corroded area, the C_{a2m} is to account for the capacitive coupling between the antenna and the base material (steel), and the L_{12r} is to account for the strip connected the left and right parts of the sensing patch, which is influenced by the slot with (w). The parameter of interest, i.e. t , can be quantified by the sensing component of C_{a2m} . Consequently, it varies along with corrosion progression, which will influence the impedance matching of the antenna, and thus can be indirectly measured via the sensing variable, i.e. AID .

C. Forward Problem Analysis for Optimization

Fig. 3 shows the simulated reflection coefficients (S_{11}) and $AIDs$ of the proposed antenna. The simulated 3-dB impedance bandwidth of the proposed antenna is larger than 50 MHz. It is

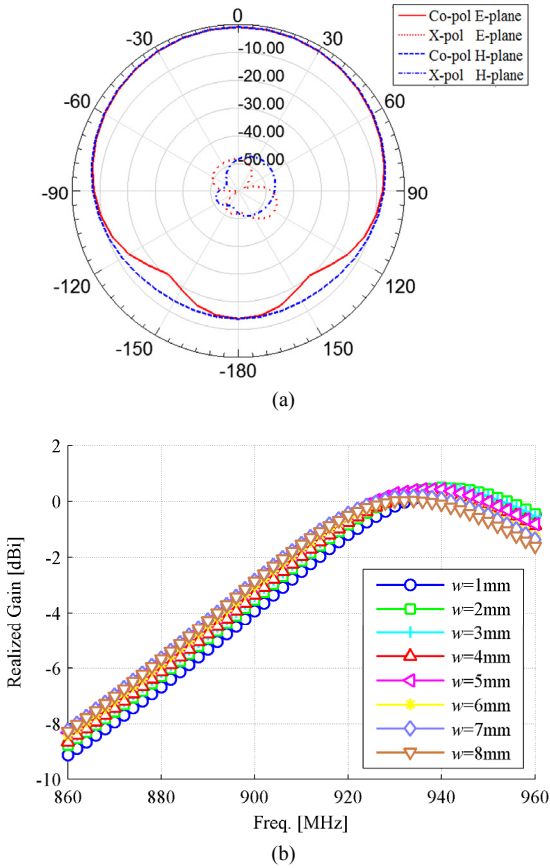


Fig. 4. (a) Simulated radiation pattern at 915 MHz when $w = 5$ mm and $t = 40$ μm (b) simulated realized gain versus frequency in the variation of w when $t = 40$ μm .

straightforward that the resonant frequency of the proposed antenna drops as an increase of h owing to the increase of the inductance (L_{cax} in Fig. 2c). Besides, because of an increase in L_{l2r} , the resonant frequency of the antenna will slightly decrease as w increases.

The simulated radiation pattern and realized gain, which have taken into consideration the impedance mismatch loss between the antenna and the tag chip [48], are depicted in Figs. 4a and 4b, respectively. The non-directional radiation pattern, resulting from the radiation in both horizontal and vertical radiating patches, makes the tag be easily identified in a wide range of spatial angles in both E (yz) and H (xz) planes (see Fig. 4a). From Fig. 4b, we see that the proposed antenna can reach its peak realized gain of 0.6 dBi at 934 MHz. The reason for the selection of w will be discussed later in this section. Nevertheless, we can find that the peak realized gain slightly decreases with the increase of w .

Fig. 5a shows the simulated input impedances of the proposed antenna sensor in the variation of t . It can be observed that a substantial change in the resistance occurs when corrosion happens. This is directly caused by a significant reduction in the resistance of R_{cal} from 1.30 Ω at the healthy state and to 1.08 Ω at the corrosion states (and maintained almost at different corrosion stages), which can be attributed to a reduction of eddy current loss at a presence of corrosion.

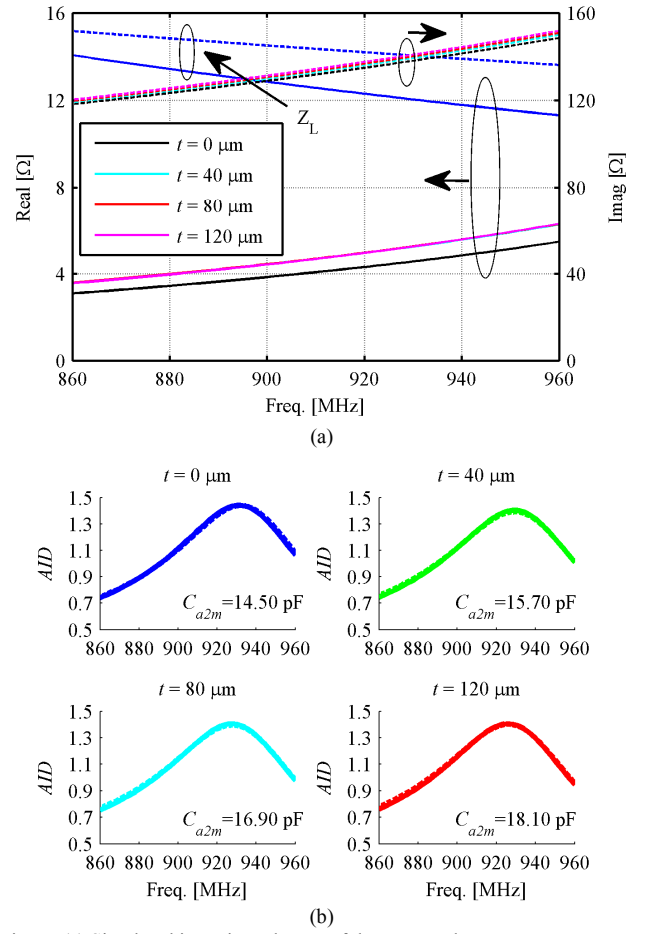


Fig. 5. (a) Simulated input impedances of the proposed antenna sensor versus frequency in the variation of t when $w = 5$ mm and (b) simulated and modeled $AIDs$ versus frequency in the variation of t when $w = 5$ mm, where solid line represents the simulated results and dash line represents the modeled ones.

Fig. 5b shows a comparison of the simulated results of $AIDs$ using full wave simulation with the results using an equivalent circuit model. A good agreement can be found, which demonstrates that the sensing principle can be reasonably reconstructed in terms of a capacitive sensing component. The increase in t leads to an increase in the displacement current (due to the cavity theory), thus rendering an increase in C_{a2m} . This drops the resonant frequency as corrosion progresses.

Fig. 6a shows a feature of single frequency (SF) directly extracted from AID . It can be found that the corrosion layer thickness produces a monotonic shift in AID in the frequency away from resonance. Therefore, SF (or RFS) can be used to act as a feature to *detect* and *characterize* the corrosion in metals. To compare the sensitivity of Ω_l and SF, a min-max normalization method is used in its feasible region to conduct a dimensionless analysis, and the results are shown in Fig. 6b. We see that the sensitivity of SF increases with the increase of w and reaches the peak value when $w = 4$ mm. However, it is not maximized near the resonant frequency (e.g. f_0), which complicates the selection of frequency points, particularly in autonomous scenarios, and also leads to a trade-off between sensing (sensitivity) and communication (distance).

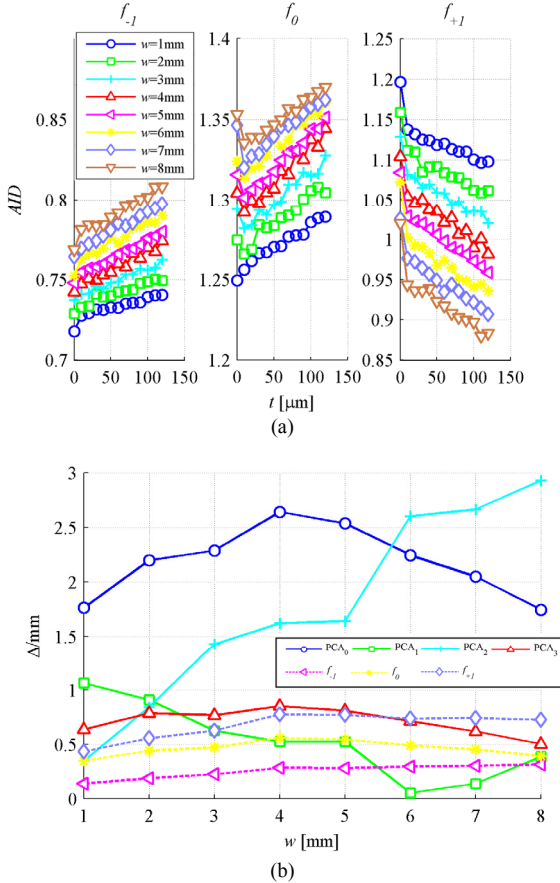


Fig. 6. (a) Simulated $AIDs$ versus t in the variation of w , where $f_{-1} = 860$ MHz, $f_0 = 915$ MHz, and $f_{+1} = 960$ MHz and (b) the sensitivities of different features, where PCA_0 and PCA_3 represent the feature of Ω_2 respectively extracted from the frequency band of 902-928 MHz and 860-960 MHz when $h = 16.0$ mm, while PCA_1 and PCA_2 represent the feature of Ω_1 extracted from the frequency band of 902-928 MHz when h is 16.5 mm and 17.0 mm, respectively.

Similarly, by comparing PCA_0 , PCA_1 , and PCA_2 , we can find that the sensitivity of the PCA method is related to the resonant frequency (or h). In contrary to the feature of SF, the PCA method uses the shape information; hence its sensitivity can be maximized even a small bandwidth is available, e.g. 902–928 MHz in this study. Therefore, to achieve an optimal trade-off between sensing and communication, the proposed antenna is tuned to resonate at 934 MHz at the healthy state, a little higher than the upper bound of the measurable frequency region. Meanwhile, a slot width of 5 mm is selected for the experimental study to ease the deployment of the tag. This is also attributed to the reason where the corrosion that happens is unknown in a priori for practical applications.

By properly choosing the antenna size and topology (radiation mode), designing the matching performance, and deploying the antenna, an acceptable trade-off between sensing (sensitivity) and communication (distance) based on UHF RFID TABS can be achieved. Based on the design, experimental studies and validation of corrosion detection and characterization are examined in the following section.

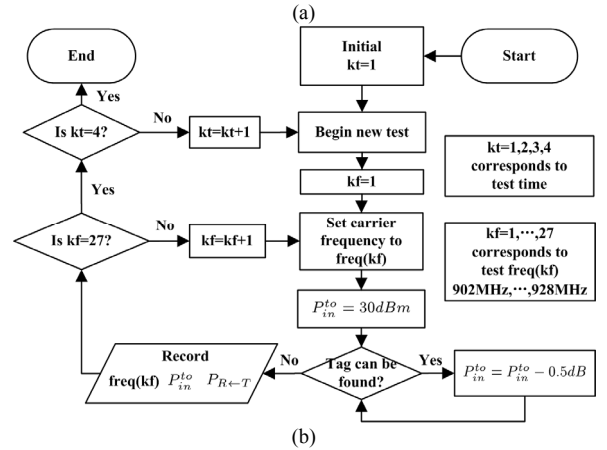
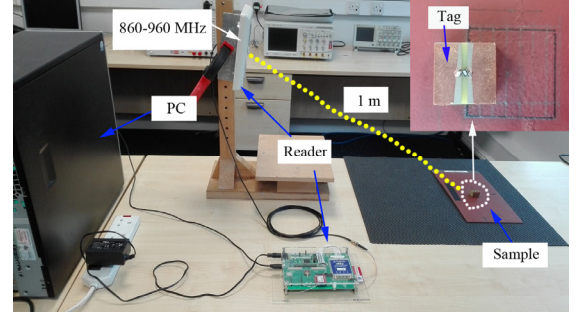


Fig. 7. (a) Hardware measurement setup and (b) software flow-chart of the RFID sensor system.

IV. MEASUREMENTS AND DISCUSSIONS

A. Experimental Setup

The forward and backscattered powers of the tag were measured using a ThingMagic Mercury xPRESS platform. The test setup and software flow-chart of the RFID sensor system are depicted in Fig. 7. The distance between the reader and tag antennas was fixed to 1 m. The reader antenna is circularly polarized (CP) with a 6 dBi gain when the radiated power was decreased from 30 dBm in a step of 0.5 dB to find the threshold power to activate the tag (P_{in}^{to}) and corresponding backscattered power ($P_{R \leftarrow T}$), hence yielding a maximum 4-W effective isotropic radiated power (EIRP). Owing to the firmware limitation, the measurement was only carried out under the operating frequency of 902–928 MHz and the reader was set to increase 1 MHz per step. The test was repeated four times for each sample for robustness.

B. Results and Discussions

In order to evaluate the performance of the proposed method, a test was carried out in a typical office in the presence of tables, boxes, metallic cabinets, and other sources of clutter [49]. Fig. 8a shows the four times measurements of P_{in}^{to} and $P_{R \leftarrow T}$ versus frequency in the variation of samples. Comparing P_{in}^{to} with $P_{R \leftarrow T}$, we can find a significant improvement in the sensitivity for the forward power to activate tag, which can be attributed to the higher power resolution of the transmitter and power-starved property in the forward link [50] while a major

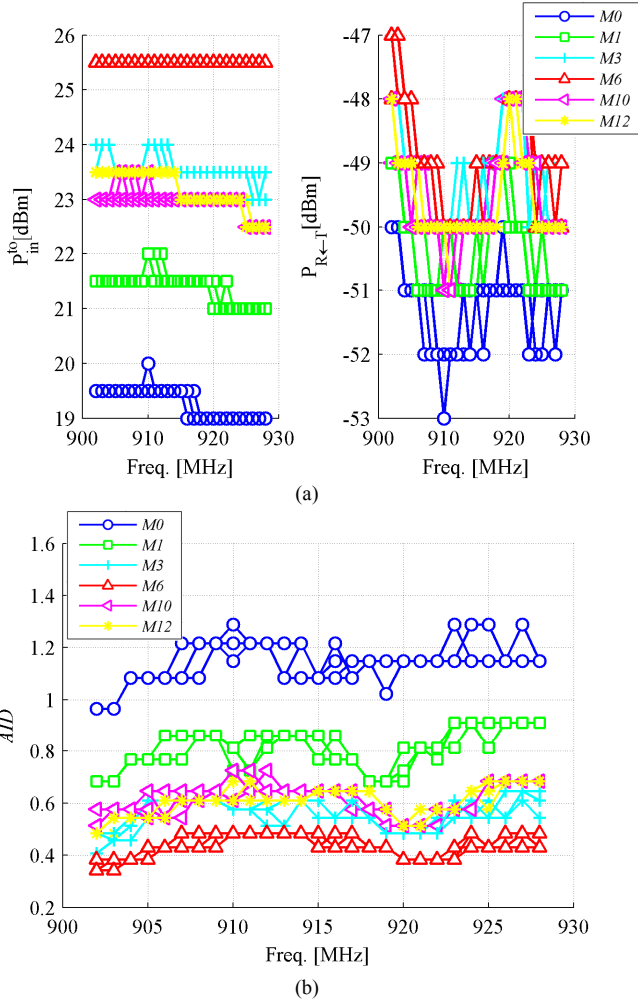


Fig. 8. The measured (a) $P_{in}^{t_0}$ and $P_{R \leftarrow T}$, and (b) AID s versus frequency in the variation of corrosion progression.

limitation for the measurement of backscattered power is the resolution of ADC in the receiver. Because of the lossy FR4 substrate and the limited measurement bandwidth, it is not easy to find the resonant frequency.

Fig. 9a shows the projection coefficients of the AID s (shown in Fig. 8b) onto the PC1 and PC2, reflecting major corrosion progression, i.e. Ω_1 and Ω_2 . Since Ω_1 represents the dominant variance (more than 97%) of corrosion signatures, it is then selected as a feature for corrosion characterization. Fig. 9b illustrates the features extracted from PCA method and SF. We can find that the sensing variable of AID through both of f_0 and Ω_1 can identify the corrosion progression in the early stage. However, Ω_1 demonstrates a better robustness. The corroded area becomes loose and flakes off as it expands, and this shows that later-stage corrosion will spread rather than increase in thickness [8]. That is, metal loss becomes dominant in the later stage and this explains why the abnormality incurs in the 10 and 12 months corrosion. The results are in line with the previous studies using vector network analyzer (VNA) and waveguides [13]. In addition, measured with laser profilometry, the average value of corrosion layer thickness for 1, 3, and 6 months

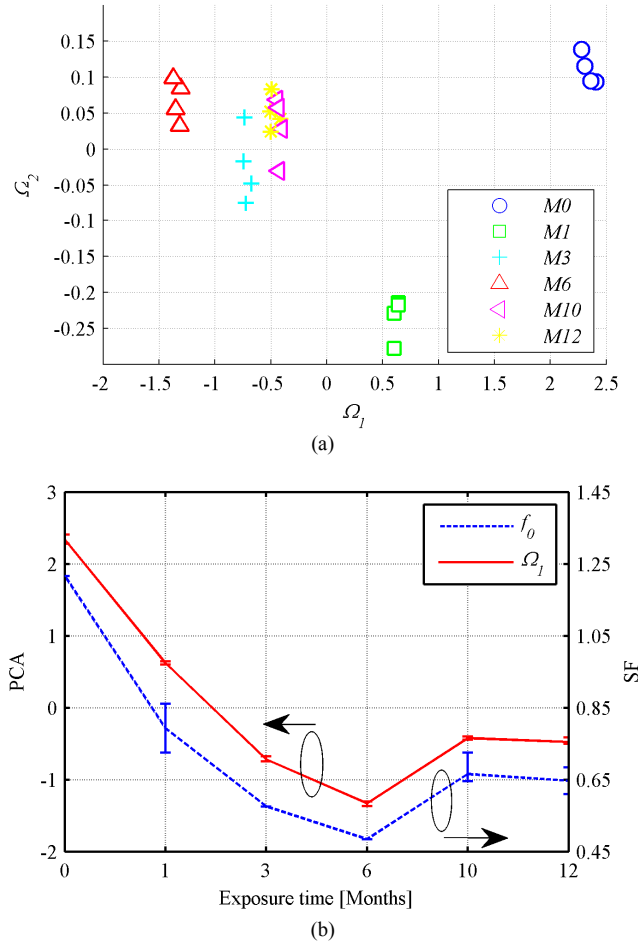


Fig. 9. (a) The distributions of Ω_1 and Ω_2 for the corrosion samples and (b) f_0 and Ω_1 versus corrosion progression, where the dash line represents the extracted feature using SF while the solid line represents the extracted feature using PCA method.

exposed corrosion samples were about 43 μm , 77 μm , and 108 μm , respectively [51]. Therefore, the proposed method of RFID sensor system using AID and PCA shows a good agreement with the previous measurements on the dedicated samples.

V. CONCLUSIONS

A 3-D UHF RFID tag antenna has been designed to sense the corrosion in metals. PCA has been used to extract sensing information by a sweep-frequency measurement of AID , which relieves the challenge in the antenna design while enhances the sensitivity and robustness. The developed RFID sensor system can successfully detect and characterize the corrosion stages and remotely measure the corrosion's information via a reader and a tag in a stand-off distance. It inherits the advantage of pulsed eddy current for NDT&E and demonstrates a cost-effective way to implement distributed monitoring. This approach has potential to bridge the gaps of NDT&E and SHM for industry application.

However, there are some limitations. The first is that one dedicated antenna is investigated for a set of dedicated samples.

The second is that the RFID grid needs to be studied for distributed monitoring. Future work will focus on how to solve these limitations and improve the RFID sensor system, which includes the design and development of more antennas for different defects and samples. Different measurement strategies from readers will be further investigated as well.

ACKNOWLEDGMENTS

The authors would like to express their gratitude to the International Paint Ltd., Tyne and Wear, U.K., for supplying the corrosion samples, to the EPSRC for the funding of the Novel Sensing Networks for Intelligent Monitoring (NEWTON) project (EP/J012343/1), and to Mr. Kevin Blacktop from Network Rail for the helpful discussion about the application of RFID sensor system along railway tracks.

REFERENCES

- [1] S. Roy, V. Jandhyala, J. R. Smith, D. J. Wetherall, B. P. Otis, *et al.*, "RFID: From Supply Chains to Sensor Nets," *Proc. IEEE*, vol. 98, pp. 1583-1592, Sep. 2010.
- [2] V. Lakafosis, A. Rida, R. Vyas, L. Yang, S. Nikolaou, *et al.*, "Progress Towards the First Wireless Sensor Networks Consisting of Inkjet-Printed, Paper-Based RFID-Enabled Sensor Tags," *Proc. IEEE*, vol. 98, pp. 1601-1609, Sep. 2010.
- [3] B. S. Cook, R. Vyas, K. Sangkil, T. Trang, L. Taoran, *et al.*, "RFID-Based Sensors for Zero-Power Autonomous Wireless Sensor Networks," *IEEE Sensors J.*, vol. 14, pp. 2419-2431, Aug. 2014.
- [4] M. Hong, Q. Wang, Z. Su, and L. Cheng, "In situ health monitoring for bogie systems of CRH380 train on Beijing-Shanghai high-speed railway," *Mech. Syst. Signal Process.*, vol. 45, pp. 378-395, Apr. 2014.
- [5] M. Safa, A. Sabet, K. Ghahremani, C. Haas, and S. Walbridge, "Rail corrosion forensics using 3D imaging and finite element analysis," *Int. J. Rail Transp.*, vol. 3, pp. 164-178, 2015.
- [6] R. A. Smith and G. R. Hugo, "Transient eddy current NDE for ageing aircraft - capabilities and limitations," *Insight*, vol. 43, pp. 14-25, Jan. 2001.
- [7] T. Hong and M. Nagumo, "Effect of surface roughness on early stages of pitting corrosion of type 301 stainless steel," *Corros. Sci.*, vol. 39, pp. 1665-1672, Sep. 1997.
- [8] Y. Z. He, G. Y. Tian, H. Zhang, M. Alamin, A. Simm, *et al.*, "Steel Corrosion Characterization Using Pulsed Eddy Current Systems," *IEEE Sensors J.*, vol. 12, Jun. 2012.
- [9] Y. Z. He, G. Y. Tian, M. C. Pan, D. X. Chen, and H. Zhang, "An investigation into eddy current pulsed thermography for detection of corrosion blister," *Corros. Sci.*, vol. 78, pp. 1-6, Jan. 2014.
- [10] H. Zhang, Y. Z. He, B. Gao, G. Y. Tian, L. X. Xu, *et al.*, "Evaluation of Atmospheric Corrosion on Coated Steel Using K-Band Sweep Frequency Microwave Imaging," *IEEE Sensors J.*, vol. 16, pp. 3025-3033, May 2016.
- [11] S. Caizzzone and E. DiGiampaolo, "Wireless Passive RFID Crack Width Sensor for Structural Health Monitoring," *IEEE Sensors J.*, vol. 15, pp. 6767 - 6774, Dec. 2015.
- [12] M. Alamin, G. Y. Tian, A. Andrews, and P. Jackson, "Corrosion detection using low-frequency RFID technology," *Insight*, vol. 54, pp. 72-75, Feb. 2012.
- [13] H. Zhang, G. Y. Tian, A. Simm, and M. Alamin, "Electromagnetic Methods for Corrosion under Paint Coating Measurement," in *Proc. SPIE 8759*, Chengdu, 2013, pp. 1-6.
- [14] M. Hasani, A. Vena, L. Sydanheimo, L. Ukkonen, and M. M. Tentzeris, "Implementation of a Dual-Interrogation-Mode Embroidered RFID-Enabled Strain Sensor," *IEEE Antennas Wireless Propag. Lett.*, vol. 12, pp. 1272-1275, 2013.
- [15] C. Occhiuzzi, S. Caizzzone, and G. Marrocco, "Passive UHF RFID antennas for sensing applications: Principles, methods, and classifications," *IEEE Antennas Propag. Mag.*, vol. 55, no. 6, pp. 14-34, Dec. 2013.
- [16] T. Bjorninen, L. Sydanheimo, L. Ukkonen, and Y. Rahmat-Samii, "Advances in antenna designs for UHF RFID tags mountable on conductive items," *IEEE Antennas Propag. Mag.*, vol. 56, no. 1, pp. 79-103, Feb. 2014.
- [17] C. Occhiuzzi and G. Marrocco, "Constrained-Design of Passive UHF RFID Sensor Antennas," *IEEE Trans. Antennas Propag.*, vol. 61, pp. 2972-2980, Jun. 2013.
- [18] C. Occhiuzzi, C. Paggi, and G. Marrocco, "Passive RFID Strain-Sensor Based on Meander-Line Antennas," *IEEE Trans. Antennas Propag.*, vol. 59, pp. 4836-4840, Dec. 2011.
- [19] J. Kim, Z. Wang, and W. S. Kim, "Stretchable RFID for Wireless Strain Sensing With Silver Nano Ink," *IEEE Sensors J.*, vol. 14, pp. 4395-4401, Dec. 2014.
- [20] M. Hasani, A. Vena, L. Sydanheimo, M. M. Tentzeris, and L. Ukkonen, "A Novel Enhanced-Performance Flexible RFID-Enabled Embroidered Wireless Integrated Module for Sensing Applications," *IEEE Trans. Compon. Packag. Manuf. Technol.*, vol. 5, pp. 1244-1252 Sep. 2015.
- [21] I. Mohammad and H. Huang, "Monitoring fatigue crack growth and opening using antenna sensors," *Smart Mater. Struct.*, vol. 19, May 2010.
- [22] I. Mohammad, V. Gowda, H. Zhai, and H. Huang, "Detecting crack orientation using patch antenna sensors," *Meas. Sci. Technol.*, vol. 23, Jan. 2012.
- [23] H. Huang, "Antenna Sensors in Passive Wireless Sensing Systems," in *Handbook of Antenna Technologies*, Z. N. Chen, Ed., ed: Springer Singapore, 2015, pp. 1-34.
- [24] V. Talla and J. R. Smith, "Hybrid analog-digital backscatter: A new approach for battery-free sensing," in *Proc. IEEE Int. Conf. on RFID*, Penang, 2013, pp. 74-81.
- [25] C. Boyer and S. Roy, "Backscatter Communication and RFID: Coding, Energy, and MIMO Analysis," *IEEE Trans. Commun.*, vol. 62, pp. 770-785, Mar. 2014.
- [26] C. Boyer and S. Roy, "Space Time Coding for Backscatter RFID," *IEEE Trans. Wireless Commun.*, vol. 12, pp. 2272-2280, May 2013.
- [27] J. D. Griffin and G. D. Durgin, "Gains For RF Tags Using Multiple Antennas," *IEEE Trans. Antennas Propag.*, vol. 56, pp. 563-570, Feb. 2008.
- [28] R. Bhattacharyya, C. Floerkemeier, and S. Sarma, "Low-Cost, Ubiquitous RFID-Tag-Antenna-Based Sensing," *Proc. IEEE*, vol. 98, pp. 1593-1600, Sep. 2010.
- [29] G. Marrocco and F. Amato, "Self-sensing passive RFID: from theory to tag design and experimentation," in *Proc. Eur. Microw. Conf.*, New York, 2009, pp. 1-4.
- [30] C. Occhiuzzi and G. Marrocco, "Uncertainty and applicability of rfid power measurements for passive sensing," in *Proc. Eur. Microw. Conf.*, Rome, 2014, pp. 255-258.
- [31] A. Sophian, G. Y. Tian, D. Taylor, and J. Rudlin, "A feature extraction technique based on principal component analysis for pulsed Eddy current NDT," *NDT&E Int.*, vol. 36, pp. 37-41, Jan. 2003.
- [32] Y. Z. He, M. C. Pan, D. X. Chen, and F. L. Luo, "PEC defect automated classification in aircraft multi-ply structures with interlayer gaps and lift-offs," *NDT&E Int.*, vol. 53, pp. 39-46, Jan. 2013.
- [33] M. Alamin, G. Y. Tian, A. Andrews, and P. Jackson, "Principal Component Analysis of Pulsed Eddy Current Response from Corrosion in Mild Steel," *IEEE Sensors J.*, vol. 12, pp. 2548-2553, Aug. 2012.
- [34] B. Gao, A. Yin, G. Y. Tian, and W. L. Woo, "Thermography spatial-transient-stage mathematical tensor construction and material property variation track," *Int. J. Thermal Sci.*, vol. 85, pp. 112-122, 2014.
- [35] G. Marrocco, "Pervasive electromagnetics: Sensing paradigms by passive RFID technology," *IEEE Wireless Commun.*, vol. 17, pp. 10-17, Dec. 2010.
- [36] P. V. Nikitin, K. V. S. Rao, and R. D. Martinez, "Differential RCS of RFID tag," *Electron. Lett.*, vol. 43, pp. 431-432, Apr. 2007.
- [37] F. Fuschini, C. Piersanti, F. Paolazzi, and G. Falciassecca, "Analytical approach to the backscattering from UHF RFID Transponder," *IEEE Antennas Wireless Propag. Lett.*, vol. 7, pp. 33-35, 2008.
- [38] G. D. Durgin, C. R. Valenta, M. B. Akbar, M. M. Morys, B. R. Marshall, *et al.*, "Modulation and Sensitivity Limits for Backscatter Receivers," in *Proc. IEEE Int. Conf. RFID*, Orlando, 2013, pp. 124-130.
- [39] D. Kuester and Z. Popovic, "How Good Is Your Tag?: RFID Backscatter Metrics and Measurements," *IEEE Microw. Mag.*, vol. 14, no. 5, pp. 47-55, July-Aug. 2013.

- [40] L. E. Mujica, J. Rodellar, A. Fernandez, and A. Guemes, "Q-statistic and T-2-statistic PCA-based measures for damage assessment in structures," *Struct. Health. Monit.*, vol. 10, pp. 539-553, Sep. 2011.
- [41] Y. Gotoh, H. Hirano, M. Nakano, K. Fujiwara, and N. Takahashi, "Electromagnetic nondestructive testing of rust region in steel," *IEEE Trans. Magn.*, vol. 41, pp. 3616-3618, Oct. 2005.
- [42] S. P. Morgan, "Effect of Surface Roughness on Eddy Current Losses at Microwave Frequencies," *J. Appl. Phys.*, vol. 20, pp. 352-362, 1949.
- [43] P. Ernst and R. C. Newman, "Pit growth studies in stainless steel foils. I. Introduction and pit growth kinetics," *Corros. Sci.*, vol. 44, pp. 927-941, May 2002.
- [44] X. Yi, T. Wu, Y. Wang, and M. M. Tentzeris, "Sensitivity Modeling of an RFID-Based Strain-Sensing Antenna With Dielectric Constant Change," *IEEE Sensors J.*, vol. 15, pp. 6147-6155, Nov. 2015.
- [45] S. A. Bokhari, J. R. Mosig, and F. E. Gardiol, "Radiation-Pattern Computation of Microstrip Antennas on Finite Size Ground Planes," *IEE Proc.-Microw. Antennas Propag.*, vol. 139, pp. 278-286, Jun. 1992.
- [46] J. Zhang and Y. L. Long, "A Novel Metal Mountable Electrically Small Antenna for RFID Tag Applications with Practical Guidelines for the Antenna Design," *IEEE Trans. Antennas Propag.*, vol. 11, pp. 5820-5829, Nov. 2014.
- [47] Monza® 4 Tag Chip Datasheet [Online]. Available: www.impinj.com
- [48] H.-D. Chen and Y.-H. Tsao, "Low-Profile PIFA Array Antennas for UHF Band RFID Tags Mountable on Metallic Objects," *IEEE Trans. Antennas Propag.*, vol. 58, pp. 1087-1092, Apr. 2010.
- [49] P. Kalansuriya, R. Bhattacharyya, and S. Sarma, "RFID Tag Antenna-Based Sensing for Pervasive Surface Crack Detection," *IEEE Sensors J.*, vol. 13, pp. 1564-1570, May 2013.
- [50] A. Bekkali, S. Zou, A. Kadri, M. Crisp, and R. Penty, "Performance Analysis of Passive UHF RFID Systems under Cascaded Fading Channels and Interference Effects," *IEEE Trans. Wireless Commun.*, vol. 14, pp. 1421-1433, Mar. 2014.
- [51] H. Zhang, "Radio Frequency Non-destructive Testing and Evaluation of Defects Under Insulation," PhD, Newcastle University, 2014.